Chemical Science

RSC Publishing

EDGE ARTICLE

View Article Online
View Journal | View Issue



Cite this: *Chem. Sci.*, 2013, **4**, 3514

# Aptamer-functionalized silver nanoclusters-mediated cell type-specific siRNA delivery and tracking†

Jingjing Li,[ab] Wenjing Wang,[a] Defang Sun,[c] Jiangning Chen,[c] Peng-Hui Zhang,[a] Jian-Rong Zhang,[a] Qianhao Min*[a] and Jun-Jie Zhu*[a]

Received 31st May 2013
Accepted 19th June 2013

DOI: 10.1039/c3sc51538a

www.rsc.org/chemicalscience

The use of small interfering RNA (siRNA) to silence target genes involved in disease has generated much excitement in the scientific community. While promising, the clinical application of RNA interference (RNAi) is still challenging in achieving effective delivery and tracking of siRNA to target cells. A new multifunctional probe comprising a cell-specific internalization aptamer, fluorescent silver nanoclusters (Ag NCs), and therapeutic siRNA was developed in one system for the specific delivery of siRNA into a target cell and for simultaneous noninvasive imaging. Different from described nanocarrier-based delivery methods which have to suffer from complicated conjugation, Ag NCs could be synthesized directly from the aptamer chimera. Sgc8c aptamer-functionalized Ag NCs as a cell-type specific siRNA delivery and imaging probe complements recent advances in PSMA aptamer-based siRNA delivery and nanomaterial-based molecular imaging. Besides, siRNA in the Ag NCs–streptavidin–siRNA complex displayed outstanding stability in both binding buffer and cell culture medium. The fluorescent intensity of biotinylated aptamer-functionalized Ag NCs was enhanced in acidic environment and no observable quenching of fluorescence occurred even after incubation for 48 h, which could benefit their usage in the intracellular environment. The facile synthetic process, good biocompatibility, excellent stability and comparable gene silencing effect with commercial reagent make it more promising for *in vivo* applications.

## Introduction

As many diseases have been disclosed to be associated with the abnormal expression of important genes, RNA interference (RNAi) is emerging as a potential approach for diagnosis and therapeutic treatment of various diseases, including obesity, heart disease, and diabetes.[1–5] RNAi can silence the expression of mRNA for a wide range of genes, such as growth factors, viral genes, oncogenes, and anti-apoptotic genes.[6,7] Small interfering RNA (siRNA, 21–23 nucleotides) is a kind of key molecule in the RNAi pathway in which it down-regulates a specific target gene by collaborating with the RNA-induced silencing complex (RISCs) and leads to the degradation of the target mRNA.[8–14] While promising, clinical application of RNAi is still challenging in achieving effective delivery and the tracking of siRNA to target cells. Liposomes, cationic polymers, viruses, inorganic nanoparticles and many other vectors have been developed to deliver siRNA into cells. Inorganic nanoparticles can enable real-time tracking of siRNA delivery, distribution and intracellular behavior with their unique electronic, optical and magnetic properties.[15–19] Bhatia *et al.*[20] and Gao and Qi[21] have achieved real-time monitoring of siRNA delivery in live cells by this type of carrier. However, these approaches may be difficult to deliver siRNA specifically to cells. Giangrande *et al.* introduced an aptamer to solve this issue.[22] They designed aptamer–siRNA chimeric RNAs, consisting of an RNA aptamer against human prostate-specific membrane antigen (PSMA) and therapeutic siRNA, to silence the target gene in tumors expressing PSMA without adverse effects on PSMA-negative tumors or normal cells. Gao and Bagalkot[23] devised quantum dot–siRNA–aptamer chimera complexes to deliver siRNA to target cells and track siRNA by fluorescence imaging.

[a]*State Lab of Analytical Chemistry for Life Science, School of Chemistry and Chemical Engineering, Nanjing University, 210093, Nanjing, P. R. China. E-mail: jjzhu@nju.edu.cn; Fax: +86-25-8357204; Tel: +86-25-8357204*

[b]*School of Medical Imaging, Xuzhou Medical College, Xuzhou, P. R. China*

[c]*State Key Laboratory of Pharmaceutical Biotechnology, School of Life Sciences, Nanjing University, 210093, Nanjing, P. R. China*

† Electronic supplementary information (ESI) available: Design of the DNA template for the synthesis of fluorescent silver nanoclusters (Fig. S1), characterization of the binding of Sgc8c or NC-Sgc8c-L5T to PTK 7 protein (Fig. S2), excitation and emission spectra of biotinylated NC-Sgc8c-L5T stabilized Ag NCs (Fig. S3), HRTEM image of NC-Sgc8c-L5T stabilized Ag NCs (Fig. S4), excitation and emission spectra of Sgc8c aptamer stabilized Ag NCs (Fig. S5), optimization of the incubation ratio between aptamer–Ag NCs, streptavidin and VEGF siRNA (Fig. S6), control experiments for confocal laser scanning microscopic images (Fig. S7), *Z*-axis scanning and DAPI nuclear staining for the characterization of the internalization of Ag NCs–streptavidin–siRNA complex (Fig. S8), and fluorescence emission spectra of Ag NCs–streptavidin–sense strand and Ag NCs–streptavidin–ds siRNA (Fig. S9). See DOI: 10.1039/c3sc51538a

However, the relatively long sequence of the anti-PSMA aptamer and easy degradation of RNA could result in lower yield and higher cost in the synthesis of the aptamer as well as increased difficulty in operation. Thus, improved delivery strategies are still in demand to monitor siRNA delivery to target cells.

Sgc8c is a cell-specific DNA aptamer which is selected against CCRF-CEM (CCL-119 T-cell, human acute lymphoblastic leukemia) through a cell-SELEX process.[24,25] It can bind human protein tyrosine kinase-7 (PTK 7) on the surface of a target lymphoblastic leukemia cell and be internalized efficiently. Ag NCs, as fluorescent nanoparticles, have excellent photostability, subnanometer size and good biocompatibility.[26,27] We previously proposed a one-step method to synthesize aptamer-functionalized silver nanoclusters (Ag NCs), employing aptamer chimera as scaffold.[28] Here we hypothesized that by combining the specific internalization ability of Sgc8c aptamer and fluorescent property of Ag NCs, the delivery of siRNA to target cells and visualization of the transport process could be achieved simultaneously.

In this study, a dual-purpose probe (Scheme 1) was designed for specific delivery of siRNA to a target cell and noninvasive imaging. Sgc8c aptamer-functionalized Ag NCs were coupled with biotinylated siRNA *via* a modular streptavidin bridge as previously reported.[29] To confirm the hypothesis, we examined the abilities of such construction to (i) specifically deliver therapeutic siRNA targeting VEGF mRNA into human cervical carcinoma (HeLa) cells; (ii) monitor the siRNA delivery by the fluorescence imaging and (iii) silence targeted gene expression without compromise. Differently from most described nanocarrier-based delivery methods which have to suffer from the complicated conjugation, Ag NCs could be synthesized directly from the aptamer chimera. The excellent stability of siRNA in the complex, good fluorescence property of Ag NCs in the acidic environment and good biocompatibility showed their potential applications in gene delivery and tracking. Such a self-tracking strategy will benefit the monitoring of future gene silencing studies both *in vitro* and *in vivo*.

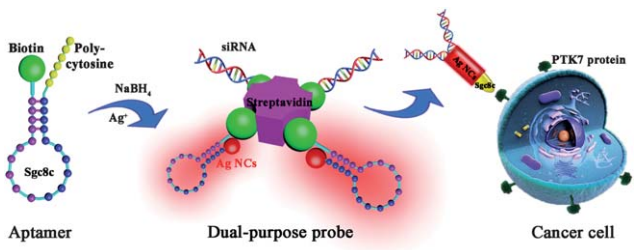


**Scheme 1** Schematic illustration of aptamer-functionalized Ag NCs-mediated cell type-specific siRNA delivery and tracking. Fluorescent Ag NCs were first synthesized through the reduction of $Ag^+$ by $NaBH_4$ with biotin-NC-Sgc8c-L5T as template. Then Sgc8c aptamer-functionalized Ag NCs were coupled with biotinylated siRNA *via* a modular streptavidin bridge in a ratio of 2 : 1 : 2 (Ag NCs : streptavidin : siRNA). Lastly, the formed complex was incubated with the target cells for specific siRNA delivery and tracking with the help of aptamer internalization and the Ag NCs fluorescent emission.

## Results and discussion

### Design of oligonucleotide scaffold

For a dual-purpose probe, the designed DNA template should not only produce fluorescent Ag NCs, but also retain the binding ability of the aptamer to target protein. We followed a universal design of an oligonucleotide scaffold for the synthesis of aptamer-functionalized Ag NCs by a previously proposed simple one-step method.[28] The sequence "NC-Sgc8c" contained a T5 loop between Sgc8c aptamer and a poly(cytosine) sequence to stabilize Ag NCs. To form the T5 loop, two guanine bases were required at the 5′ end of Sgc8c.[28] However, this modification of NC-Sgc8c could lead to the loss of an "A–T" base-pair in the predicted secondary structure, compared to intact Sgc8c (Fig. S1 in ESI†). Because of the important role of the loop-stem in structure and conformation stabilization for target binding,[27] we redesigned NC-Sgc8c to bear the same secondary structure as Sgc8c. The predicted structure of the redesigned DNA template (designated NC-Sgc8c-L5T in this work) is consistent with that of Sgc8c. To confirm the similar binding affinity to Sgc8c, we first performed the circular dichroism experiment to study the secondary structure of NC-Sgc8c-L5T. Fig. S2a† shows the CD spectra of Sgc8c and NC-Sgc8c in the presence of 0.1 M NaCl. It is known that the "folded" quadruplexes have a CD spectrum characterized by a positive ellipticity maximum at 295 nm and a negative minimum at 265 nm.[30] After modification, the secondary structure of NC-Sgc8c-L5T displayed a "folded" type. We further used 4% native PAGE to compare the two sequences. Proteins extracted from CCRF-CEM and HeLa cell lysates were incubated with fluorescently labeled Sgc8c or NC-Sgc8c-L5T at 37 °C for 1 h before loading. The gel image indicated that NC-Sgc8c-L5T and Sgc8c are bound to the target protein with comparable affinities (Fig. S2b†). It should be noted that HeLa cells also express PTK 7 protein.[31] (Lane 3 and Lane 4 in Fig. S2b†). The different migration rates of NC-Sgc8c-L5T-PTK 7 complex (Lane 2 and Lane 3, Fig. S2b†) and Sgc8c-PTK 7 complex (Lane 1 and Lane 4) could be attributed to the length of the two sequences. These data combining with flow cytometry experiments (Fig. S2c†) supported that this designed oligonucleotide scaffold, NC-Sgc8c-L5T, possessed specific affinity to its aptamer target, which was crucial to the following siRNA delivery.

### Preparation of biotinylated NC-Sgc8c-L5T-stabilized Ag NCs

Silver nanoclusters are generally produced by the reduction of a mixture of DNA scaffold and silver nitrate by sodium borohydride. To our surprise, Ag NCs stabilized by NC-Sgc8c-L5T presented a much higher fluorescence output than those stabilized by NC-Sgc8c (Fig. 1a). To obtain the optimal fluorescent property, the ratio of oligonucleotide to $Ag^+$ was varied from 1 : 1 to 72 : 1, and the best result came from 30 : 1, *i.e.* 2 : 1 for nucleobase : $Ag^+$ (Fig. 1b), which was in agreement with the phenomenon reported previously.[32–34] Here we used VEGF siRNA as a model to construct the Ag NCs–streptavidin–siRNA complex. In this system, biotin-labeled NC-Sgc8c-L5T was used to synthesize Ag NCs as the template at first. While

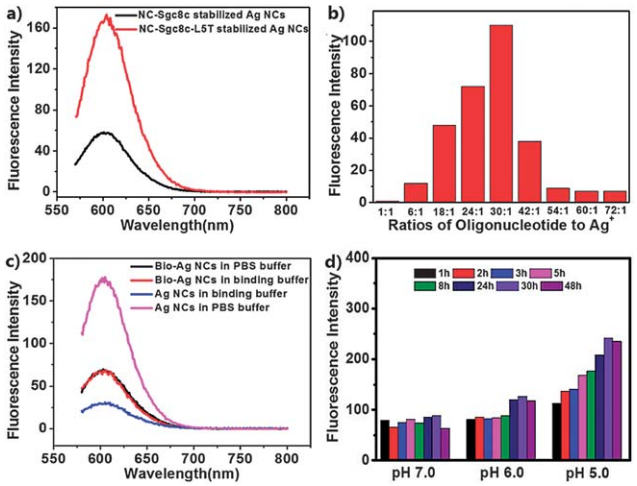


**Fig. 1** (a) Fluorescence emission spectra of Ag NCs templated by NC-Sgc8c or NC-Sgc8c-L5T; (b) effect of oligonucleotide to $Ag^+$ ratio on the fluorescence intensity of NC-Sgc8c-L5T stabilized Ag NCs; (c) fluorescence emission spectra of biotinylated or non-biotinylated Ag NCs in PBS or binding buffer solution; (d) fluorescence stability of biotinylated Ag NCs in binding buffer solution over a range of pH. Excitation wavelength: 565 nm.

the biotinylation of NC-Sgc8c-L5T compromised the fluorescence emission of Ag NCs in PBS buffer (Fig. 1c, purple and black line), the fluorescence quenching effect by ions was attenuated. In the binding buffer, the fluorescence emission intensity of biotinylated Ag NCs was 2-fold larger than the non-biotinylated ones (Fig. 1c, red and blue color) and the fluorescent property of biotinylated Ag NCs was considerably stable in the binding buffer over a range of pH even over 48 h (Fig. 1d). The fluorescent stability could benefit the visualization of siRNA transport into cells during transfection process. The size and morphology of the prepared Ag NCs were characterized by high-resolution transmission electron microscopy (HRTEM) and dynamic light scattering (DLS). As shown in Fig. S4,† an average size of Ag NCs with good crystallinity was about 3.0 nm, which was a little smaller than the hydrodynamic diameter (4.6) nm, determined by DLS. As expected, the hydrodynamic diameter is a bit larger than the diameter estimated from a visual examination of HRTEM since the hydrodynamic diameter is the sum of the core size and the thickness of adsorbed molecules layer.[35] It should be mentioned that the Sgc8c aptamer itself could also be used as the template to synthesize fluorescent Ag NCs, but the fluorescence emission is much weaker than those stabilized by biotin-NC-Sgc8c-L5T (Fig. S5†). So the observed fluorescence emission in our case mainly came from biotinylated NC-Sgc8c-L5T-stabilized Ag NCs.

## Formation and characterization of Ag NCs-streptavidin–siRNA complex

Sgc8c aptamer-functionalized Ag NCs were coupled with biotinylated siRNA *via* a modular streptavidin bridge. Biotinylated siRNA and biotinylated NC-Sgc8c-L5T-stabilized Ag NCs were incubated with streptavidin in a 2 : 1 : 2 ratio for 15 min at room temperature. Gel-shift analysis confirmed the formation of this complex (Fig. 2a). Compared with Lane 1 and Lane 2, the complex band presented a much slower migration rate (Lane 3). Additionally, siRNA and aptamer–Ag NCs bands were almost negligible after incubation, which indicated the successful formation of the complex. On the other hand, in the absence of biotinylated siRNA, a weak band with a faster migration rate was present, which might have came from streptavidin–Ag NCs or streptavidin–2 Ag NCs complex (Lane 4). In the absence of biotinylated Ag NCs, the complex band displayed a similar migration rate with that of Lane 3, which indicated the formation of streptavidin–4 siRNA complex because of the similar migration rate of Ag NCs and siRNA (Lane 5). But no streptavidin–4 Ag NCs complex was formed in Lane 4, which might be ascribed to the steric hindrance of the Ag NCs. The optimization of the incubation ratio between aptamer–Ag NCs, streptavidin and VEGF siRNA as well as the influence of incubation ratios on the gene silencing effect were also investigated and the optimal ratio was 2 : 1 : 2 (Fig. S6† and 6).

Since RNA is easily degraded, we further studied the stability of siRNA in the complex. As shown in Fig. 2b, the siRNA band was weakened after incubation for 5 h in the binding buffer (3) and incubation for 3 h in cell culture medium (4). However, the intensity of the Ag NCs–streptavidn–siRNA bands were almost unchanged over 6 h both in binding buffer (1) and cell culture medium (2), showing the good stability of siRNAs in the complex. It was reported that nanoparticles had the ability to interact with enzymes in a unique and often multivalent manner, which could resist enzymatic degradation of oligonucleotides attached to them.[36,37] Therefore, the improved stability of siRNA in the complex here might be attributed to the protection of siRNA from degradation by Ag NCs.

## MTT assay

The biocompatibility of the probe deserves special attention for potential clinical application because the cytotoxicity of foreign

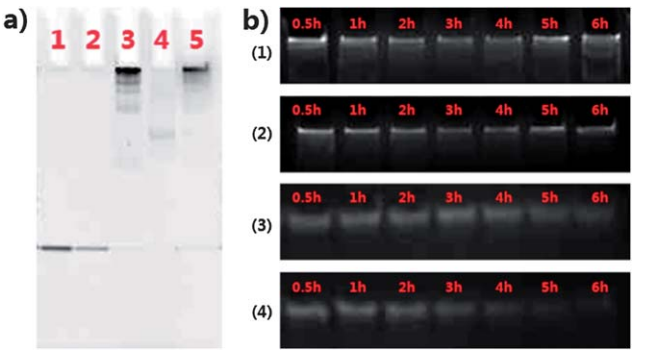


**Fig. 2** (a) Gel-shift analysis of Ag NCs–streptavidin–siRNA complex, as visualized with ethidium bromide. Lane 1: biotinylated siRNA; Lane 2: biotinylated aptamer–Ag NCs; Lane 3: Ag NCs–streptavidin–siRNA complex; Lane 4: biotinylated aptamer–Ag NCs conjugated with streptavidin; Lane 5: biotinylated siRNA conjugated with streptavidin. (b) The stability of siRNA of the complex and siRNA alone in binding buffer (1,3) or cell culture medium (2,4) with different incubation time.

materials in living systems is an important point of concern.[38] No matter how good polymers such as poly(L-lysine) (PLL) and poly(ethylenimine) (PEI) or inorganic nanoparticles such as quantum dots are in nonviral gene delivery, the major drawback falls in their toxicity.[39] With concern for this issue, we examined the cytotoxicity of NC-Sgc8c-L5T-stabilized Ag NCs using MTT ((3,4,5-dimethylthiazol-2-yl)-2,5-diphenyltetrazolium bromide) assay. HeLa, NIH-3T3 and RAW 264.7 cells were exposed to aptamer–Ag NCs ranging from 5 nM to 2 μM and equal concentrations of lipofectamine 2000 in the following gene silencing. As shown in Fig. 3, no significant cellular toxicity of NC-Sgc8c-L5T-stabilized Ag NCs was observed, demonstrating good cytocompatibility of Ag NCs, but a little toxicity for lipofectamine 2000. The concentration of 2 μM NC-Sgc8c-L5T-templated Ag NCs was thus chosen for the following imaging experiments.

### Fluorescence tracking of the internalization of Ag NCs–streptavidin–siRNA complex

The specific cellular-internalization of the constructed Ag NCs–streptavidin–siRNA complex was tracked by the fluorescence emission of aptamer–Ag NCs. HeLa cells expressing PTK 7 protein were incubated with aptamer–Ag NCs and non-binding aptamer–Ag NCs, respectively. Ramos cells which were deficient in PTK 7 protein were treated with 2 μM aptamer–Ag NCs for 2 h before being imaged by fluorescence confocal microscopy as a control. As shown in Fig. 4, biotinylated NC-Sgc8c-L5T-stabilized Ag NCs could be internalized into HeLa cells easily while internalization was not observed in the case of non-binding aptamer–Ag NCs and Ramos control cells (Fig. S7B†), indicating its cell-specificity. The fluorescence was mainly from the cell membrane at first (Fig. 4a), and later on we could observe the fluorescence emitted inside the cell and in part from nucleus (from Fig. 4b to c and S8b†).

Then the fate of the Ag NCs–streptavidin–siRNA complex was also investigated. Similar to aptamer–Ag NCs, the presence of siRNA and streptavidin did not interfere with internalization process and the complex could be successfully internalized into HeLa cells (Fig. 5). Three-dimensional images of entire

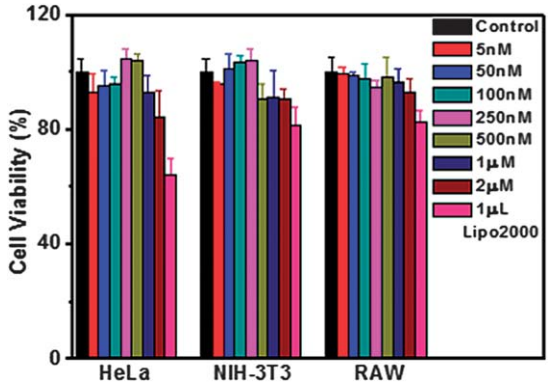


**Fig. 3** HeLa human cervical carcinoma cell viability, NIH-3T3 mouse fibroblast cell viability and RAW 264.7 murine macrophage viability after 24 h exposure to various amounts of NC-Sgc8c-L5T-templated Ag NCs and lipofectamine 2000.

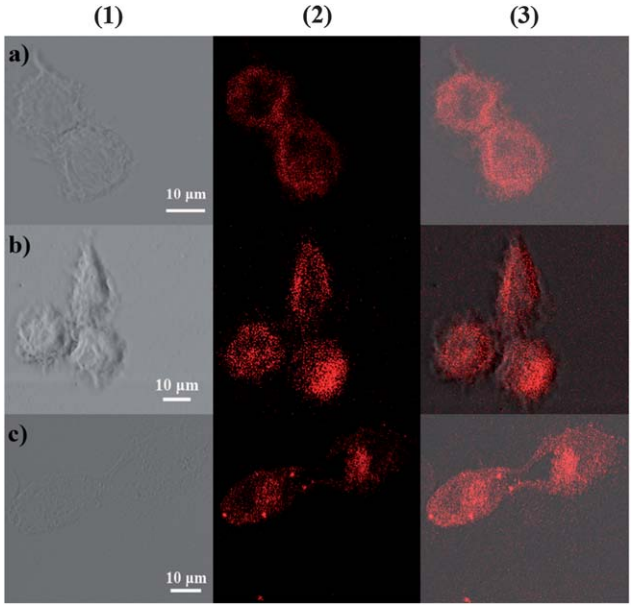


**Fig. 4** Confocal laser scanning microscopic image of HeLa human cervical carcinoma cells incubated with biotin-NC-Sgc8c-L5T-stabilized Ag NCs at 37 °C at different time points: 1 h (a), 3 h (b), and 5 h (c). (1) Bright-field images; (2) Ag NCs fluorescence images; (3) overlapped corresponding fluorescence images and bright-field images. The Ag NCs were excited with UV.

cells after the internalization of the Ag NCs–streptavidin–siRNA complex confirmed the presence of the complex inside cells as well (Fig. S8a†). Additionally, by further comparing the phase-contrast image with nuclear DAPI staining (Fig. S8b†), we found that the intracellular Ag NCs were mainly accumulated in the nuclei eventually, which was consistent with a

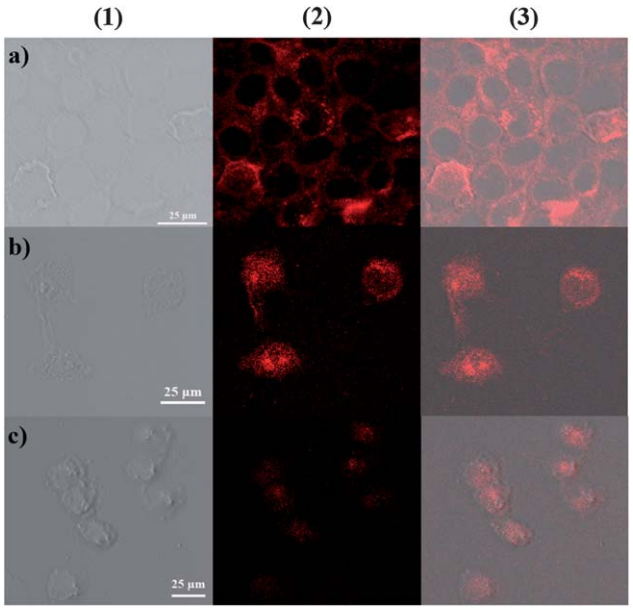


**Fig. 5** Confocal laser scanning microscopic image of Ag NCs–streptavidin–siRNA complex at 37 °C at different time points: 1 h (a), 3 h (b), and 5 h (c). (1) Bright-field images; (2) Ag NCs fluorescence images; (3) overlapped corresponding fluorescence images and bright-field images. The Ag NCs were excited with UV.

previous report.[40] Since it was an Sgc8c aptamer-mediated endocytic process for the internalization of the complex,[41] we hypothesize the possible internalization course of Ag NCs–streptavidin–siRNA complex: first into endosome by endocysis, then RNAi pathway into cytoplasm, and eventually into the nucleus. But up to now, we still have no idea about the exact life cycle of the complex from endosome to cytoplasm. These data substantially suggested that the Ag NCs–streptavidin–siRNA complex could be used as a dual-purpose probe for both cellular delivery and imaging. The fluorescence intensity of Ag NCs–streptavidin–siRNA decreased after 5 h incubation (Fig. 5c), but not in the control of biotin-NC-Sgc8c-L5T stabilized Ag NCs alone (Fig. 4c). Considering the fluorescence enhancement and stability of Ag NCs in acidic environment (Fig. 1d), reduced fluorescent intensity might came from the hybridization of siRNA with its target mRNA in RNAi pathway.[42] To test our hypothesis, additional experiments were designed. In RNA interference, an antisense strand will be first separated from the sense strand to be incorporated into the RNA-induced silencing complex (RISC).[43] So we wonder whether such separation will influence the fluorescence emission of Ag NCs. Biotin-NC-Sgc8c-L5T-stabilized Ag NCs were conjugated with the biotinylated antisense strand and biotinylated ds siRNA, respectively. As shown in Fig. S9,† the absence of the antisense strand from the Ag NCs caused a decrease of fluorescence intensity, which might indicate the occurrence of the gene silencing process. Such fluorescence sensitivity of DNA-stabilized Ag NCs to the oligonucleotide surroundings is a benefit for their applications in DNA or RNA sensing and an Ag NC-based "light-up" *in situ* assay is undergoing in our group.

### Gene silencing evaluation of Ag NCs–streptavidin–siRNA complex

At last, the therapeutic effect by targeted delivery of VEGF siRNA *via* the Ag NCs–streptavidin–siRNA complex was evaluated. HeLa cells were transfected with the complex containing 20 pmol VEGF siRNA and the VEGF mRNA and VEGF protein expression levels were determined at two days post-transfection by qRT-PCR assay and Human VEGF ELISA Kit. Aptamer–Ag NCs, a complex containing VEGF siRNA and negative control siRNA (Ag NCs–streptavidin–VEGF siRNA, Ag NCs–streptavidin–NC siRNA), commercially available lipoplex (Lipo2000-VEGF siRNA complex, Lipo2000-NC siRNA), Ag NCs, streptavidin and VEGF siRNA in different ratios, VEGF siRNA–streptavidin–Ag NCs stabilized by biotin-NC-L5T and VEGF siRNA–streptavidin–Ag NCs stabilized by biotin-NC-L5T in the presence of Sgc8c aptamer and non-binding aptamer–Ag NCs–streptavidin–VEGF siRNA in a ratio of 2 : 1 : 2 were included (Fig. 6). Only negligible inhibition of VEGF expression was observed in the control groups. Sgc8c aptamer-mediated transfection displayed comparable suppression of VEGF, compared to that by Lipo2000, suggesting non-compromised efficacy of siRNA within the complex. The gene could only be silenced when both VEGF siRNA and Sgc8c aptamer functionalized Ag NCs were present as a whole.

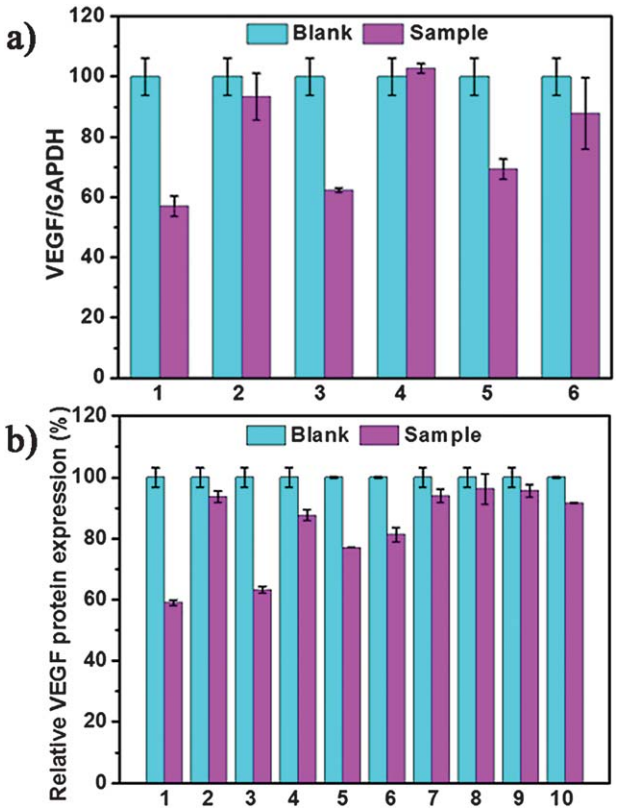


**Fig. 6** Gene silencing effect of aptamer-functionalized Ag NCs-based siRNA delivery on VEGF mRNA expression (a) and VEGF protein expression (b) in HeLa cell lines. Cells were treated with (1) Ag NCs–streptavidin–VEGF siRNA in a ratio of 2 : 1 : 2. At the same time, cells were treated with (2) Ag NCs–streptavidin–NC siRNA, (3) Lipo2000-VEGF siRNA, (4) Lipo2000-NC siRNA complex, (5) Ag NCs–streptavidin–VEGF siRNA in a ratio of 1 : 1 : 3, (6) Ag NCs–streptavidin–VEGF siRNA in a ratio of 3 : 1 : 1, (7) aptamer–Ag NCs, (8) siRNA–streptavidin–Ag NCs stabilized by biotin-NC-L5T, (9) siRNA–streptavidin–Ag NCs stabilized by biotin-NC-L5T in the presence of Sgc8c aptamer and (10) non-binding aptamer–Ag NCs–streptavidin–VEGF siRNA in a ratio of 2 : 1 : 2 as controls. Silencing efficiency was evaluated by VEGF quantification after 48 h post-transfection. The VEGF knock-down data was normalized with the expression levels of VEGF in the non-treated HeLa-VEGF cells (blank).

## Conclusions

In summary, we have developed a new multifunctional probe comprising a cell-specific internalization aptamer, fluorescent Ag NCs, and therapeutic siRNA in one system. Sgc8c aptamer-functionalized Ag NCs as a cell-type specific siRNA delivery and imaging probe complements recent advances in PSMA aptamer-based siRNA delivery and nanomaterial-based molecular imaging. The excellent fluorescent stability of the biotinylated aptamer-functionalized Ag NCs in buffers of pH ranging from 5.0 to 7.0, combined with the enhanced stability of siRNA in the complex enabled their promising application in the intracellular siRNA delivery and tracking. Additionally, due to the tunable fluorescence emission wavelength of Ag NCs by the DNA template sequence, delivery and monitoring of multiple siRNAs with different colours could also be potentially realized.

## Experimental

### Chemicals and materials

Silver nitrate (99+%), sodium borohydride ($NaBH_4$, powder, 98%), disodium hydrogen phosphate, sodium chloride, magnesium chloride, calcium chloride, glucose, paraformaldehyde and glycerol were purchased from Nanjing Chemical Reagents Factory (Nanjing, China). Dulbecco's phosphate buffered saline was purchased from Sigma. Cell cultures including HDMEM, RPMI 1640 and α-MEM medium were obtained from Nanjing KenGen Biotech Co. Ltd. (Nanjing, China). Cell lysis solution, diethylpyrocarbonate (DEPC) and human VEGF ELISA Kit were purchased from Beyotime Institute of Biotechnology (Nanjing, China). LipofectamineTM 2000 and Opti-MEM were obtained from Invitrogen Corporation. Reagents for polyacrylamide gel electrophoresis, including 40% acrylamide mix solution, ammonium persulfate (APS), 1,2-bis-(dimethylamino)ethane (TEMED) and ethidium bromide (EB) were purchased from Shanghai Sangon Biotechnology Co. Ltd. (Shanghai, China). All DNA oligos were synthesized and purified by Shanghai Sangon Biotechnology Co. Ltd. (Shanghai, China). siRNAs were obtained from GenePharma Co. Ltd. (Shanghai, China). The DNA and siRNA sequences are as follows:

Sgc8c: 5′-ATC TAA CTG CTG CGC CGC CGG GAA AAT ACT GTA CGG TTA GA-3′.

NC-Sgc8c: 5′-CCC CCC CCC CCC TTT TTGG ATC TAA CTG CTG CGC CGC CGG GAA AAT ACT GTA CGG TTA GA-3′.

NC-Sgc8c-L5T: 5′-CCC CCC CCC CCC TTT TTG GA ATC TAA CTG CTG CGC CGC CGG GAA AAT ACT GTA CGG TTA GA-3′.

NC-L5T: 5′-CCC CCC CCC CCC TTT TT-3′.

Non-binding aptamer: 5′-CCC TTA ATC CCC TAT AAT AAA TTT TAA TTTTT GGT TGG TGT GGT TGG-3′.

Human VEGF siRNA sense sequence: 5′-GGA GUA CCC UGA UGA GAU CdTdT-3′ antisense sequence: 5′-GAU CUC AUC AGG GUA CUC CdTdT-3′.

Negative control siRNA sense sequence: 5′-UUC UCC GAA CGU GUC ACG UTT-3′ antisense sequence: 5′-ACG UGA CAC GUU CGG AGA ATT-3′.

All other chemicals involved in this work were analytical-grade. All aqueous solutions were prepared in DEPC treated ultrapure water (≥18 MΩ, Milli-Q, Millipore).

### Apparatus and characterization

Fluorescence measurements were carried out using an RF-5301 PC (Shimadzu, Kyoto, Japan). The excitation/emission wavelengths were set at 565 nm/605 nm. Circular dichroism (CD) spectra were obtained on a J-810 spectropolarimeter. Fluorescence gel imaging was carried out using a Bio-Rad imaging system (serial no. 76s/06725). The secondary structure of DNA oligos were analyzed by OligoAnalyzer 3.1 (free online software from IDT). Flow cytometric analysis was carried out using Cytomics FC 500 MCL (Beckman Coulter, USA). qRT-PCR was performed at ABI 7300 Sequence Detection System. Fluorescence imaging and *Z*-axis scanning were performed with a confocal laser microscope (TCS SP5, Leica, Germany).

### Cells and cell culture conditions

HeLa cells (human cervical carcinoma) and NIH-3T3 mouse fibroblast cells were obtained from Nanjing KenGen Biotech Co. Ltd. (Nanjing, China) and seeded in HDMEM medium (Gibco, Grand Island, NY) supplemented with 10% fetal calf serum (FCS, Sigma), penicillin (100 μg $mL^{-1}$), and streptomycin (100 μg $mL^{-1}$) and incubated under 5% $CO_2$, 37 °C. CCRF-CEM (CCL-119 T-cell line, human acute lymphoblastic leukemia cell) and RAW 264.7 murine macrophage were purchased from the Cell Bank of the Chinese Academy of Sciences (Shanghai, China). Ramos cells (CRL-1596, B-cell, human burkitt's lymphoma) were from Shanghai Bioleaf Biotech Co. Ltd. (Shanghai, China). CCRF-CEM and Ramos cell lines were cultured similarly with HeLa cells except that HDMEM was replaced by RPMI 1640 medium and α-MEM medium for RAW 264.7 murine macrophage. The cells were harvested from 90% confluent cell culture plates and the cell density was determined by use of a Petroff-Hausser cell counter prior to experiments. The binding buffer used for aptamer internalization was 4.5 g $L^{-1}$ glucose and 5 mM $MgCl_2$ in Dulbecco's phosphate buffered saline with calcium chloride and magnesium chloride.

### Preparation of Ag NCs–streptavidin–siRNA complex

DNA-stablized Ag NCs were synthesized according to procedures described elsewhere with slight modifications.[34,44,45] Briefly, 12 μL of 250 μM NC-Sgc8c-L5T was mixed with 36.8 μL 20 mM phosphate (pH 7.0) buffer, and then 8.8 μL 10 mM $AgNO_3$ was added to reach a nucleobase to $Ag^+$ molar ratio of 2 : 1. After being chilled on ice for 15 min, the mixture was reduced by quickly adding 22.4 μL of 4 mM $NaBH_4$, followed by vigorous shaking for 1 min. The reaction was kept at 4 °C before use. (Note: the $NaBH_4$ solution must be freshly prepared prior to use.) Non-binding aptamer stabilized Ag NCs were synthesized by the same method.

The Ag NCs–streptavidin–siRNA complex was assembled by using biotin-labeled double-stranded siRNA and aptamer–Ag NCs to conjugate with streptavidin in a ratio of 2 : 1 : 2 (Ag NCs : streptavidin : siRNA). The complex was allowed to equilibrate for a minimum of 10 min at room temperature and then was stored on ice until use. For fluorescence imaging, Ag NCs–streptavidin–siRNA complex was added into the binding buffer at a final concentration of 2 μM.

### Circular dichroism measurement

In order to study the secondary structure of NC-Sgc8c-L5T, the CD spectra of Sgc8c and NC-Sgc8c-L5T in the presence of 0.1 M NaCl were analyzed on a J-810 spectropolarimeter. The CD spectra were recorded from 220 to 500 nm and the corresponding parameter settings were as follows: scanning speed 50 nm $min^{-1}$, response time 0.25 s, bandwidth 1.0 nm, and 2 times accumulation.[46] The concentration of DNA samples were 12 μM.

### Polyacrylamide gel electrophoresis analysis

4% native polyacrylamide gel was used to examine the binding of NC-Sgc8c-L5T to PTK7 protein. Proteins extracted from

CCRF-CEM and HeLa cell lysates were incubated with FAM-labeled Sgc8c or FAM-labeled NC-Sgc8c-L5T at 37 °C for 1 hour, respectively. Then, the complex was resolved by gel electrophoresis on 4% polyacrylamide at 100 V for 90 min and recorded directly by fluorescence gel imaging system.

12% polyacrylamide gel was employed for the characterization of the fabricated Ag NCs–streptavidin–siRNA complex and the stability of the siRNA of the complex and siRNA alone in binding buffer or cell culture medium over 6 h. Electrophoresis was carried out at 100 V for 1 hour at room temperature. After separation, the gel was stained with ethidium bromide and imaged by fluorescence gel imaging system.

### Flow cytometric analysis

To study the binding ability of NC-Sgc8c-L5T-stabilized Ag NCs with the target cells, NC-Sgc8c-L5T-stabilized Ag NCs were incubated with HeLa cells cultured in a 6-well plate for 2 h at 37 °C. After incubation, cells were washed with PBS, lysed and redispersed in PBS buffer for the following flow cytometry analysis. NIH-3T3 mouse fibroblast cells were used as control.

### MTT assay

HeLa cells, NIH-3T3 mouse fibroblast cells and RAW 264.7 murine macrophage were plated in 96-well plates at a density of $1 \times 10^4$ cells per well in 200 μL of culture medium and incubated for 24 h at 37 °C before exposure to aptamer–Ag NCs and Lipo2000. Prior to the exposure, synthesized Ag NCs were centrifuged for 100 min at 10 000 rpm through a 3 kDa cutoff filter to remove unbound $Ag^+$ from aptamer–Ag NCs. Cells were treated with a range of aptamer–Ag NCs concentrations (5 nM, 50 nM, 100 nM, 250 nM, 500 nM, 1 μM and 2 μM) or 1 μL Lipo2000 and media were removed after treatment. Then the cells were washed twice with PBS buffer before the addition of HDMEM containing MTT (5 mg $mL^{-1}$) (HeLa and NIH-3T3 cells) or α-MEM containing MTT (5 mg $mL^{-1}$) (RAW 264.7 murine macrophage) and further incubated at 5% $CO_2$, 37 °C for another 4 h. At last, media containing MTT were replaced by 100 μL of dimethyl sulfoxide (DMSO) to solubilize the formazan crystals precipitates. The plate was shaken for 15 min at 37 °C before measurements of optical absorbance at 492 nm on a model 680 microplate reader (Bio-Rad). The cell viability was determined relative to the untreated control cells.[47]

### Confocal laser microscopy assay and *Z*-axis scanning

The internalization of aptamer–Ag NCs and the Ag NCs–streptavidin–siRNA complex was examined with confocal laser microscopy by the fluorescence of Ag NCs. HeLa cells ($1 \times 10^4$ cells) were seeded onto a 12 mm sterile coverslip in a 24-well plate. After 24 h, cells were transfected with 2 μM aptamer–Ag NCs, Ag NCs–streptavidin–siRNA complex for 1–5 h at 37 °C after washing three times with phosphate-buffered saline (PBS). The cells were then washed with cold PBS three times and fixed for 20 min in 200 μL of 3.7% paraformaldehyde. After washing three times with PBS, the side of the coverslip with fixed cells was topped by a glass slide with a 10 μL drop of 50% glycerol/PBS (V/V). The glass slide was inverted and placed above a 20× objective on the confocal microscope. The Ag NCs were excited with UV. Ramos cells were cultured in special Petri dish which could be used for confocal laser scanning directly. They were treated with the same concentration of aptamer–Ag NCs and the fluorescence imaging was recorded as a control. Non-binding aptamer-stabilized Ag NCs were also incubated with HeLa cells as a control.

*Z*-Axis scanning was used to further examine the internalization of aptamer–Ag NCs.[48] Parameters involved in the *Z*-axis scanning included the beginning and ending *Z*-value for the sample, thickness of the sample, and number of optical sections within the volume. Micrographs were taken while the focal plane was moved in incremental steps from the coverslip bottom up to the top of the cells.

For nucleus staining, HeLa cells ($1 \times 10^4$ cells) were seeded in special Petri dish. After 24 h, cells were transfected with 2 μM aptamer–Ag NCs for 5 h at 37 °C after washing three times with phosphate-buffered saline (PBS). The cells were then washed with cold PBS three times and nucleus stained with 4′6-diamidino-2-phenylindole dihydrochloride (DAPI). The cells were further washed three times with PBS buffer for confocal laser scanning after 10 min.

### *In vitro* transfection

For *in vitro* transfection studies, $1 \times 10^4$ HeLa cells per well were cultured in a 24-well plate. After incubation for 24 h, the culture medium was removed and cells were washed with the binding buffer three times. VEGF siRNA (20 pmol) was conjugated with aptamer–Ag NCs by streptavidin in 100 μL binding buffer. The Ag NCs–streptavidin–VEGF siRNA complex was left at ambient temperature for 15 min and then added to treat the cells. After 5 h transfection at 37 °C, the transfection solution was replaced by a fresh culture medium. At last, the medium was collected for VEGF ELISA assay after further incubation for 48 h. The VEGF secreted from the cells was quantified using a human VEGF ELISA Kit according to the manufacturer's instructions. Aptamer–Ag NCs, Ag NCs–streptavidin–NC siRNA complex, Lipo2000-VEGF siRNA, Lipo2000-NC siRNA, VEGF siRNA–streptavidin–Ag NCs stabilized by biotin-NC-L5T, VEGF siRNA–streptavidin–Ag NCs stabilized by biotin-NC-L5T in the presence of Sgc8c aptamer, Ag NCs–streptavidin–VEGF siRNA in a ratio of 1 : 1 : 3, Ag NCs–streptavidin–VEGF siRNA in a ratio of 3 : 1 : 1, and non-binding aptamer–Ag NCs–streptavidin–VEGF siRNA in a ratio of 2 : 1 : 2 were also performed under the same condition as the controls.

### RNA isolation and VEGF mRNA detection by qRT-PCR

Total cellular RNAs were extracted from HeLa cells using Trizol reagent (Invitrogen) according to manufacturer's protocols. The first-strand cDNA was generated by PrimeScript RT Master Mix Kit (Takara). Quantitative PCR was done with an ABI 7300 Sequence Detection System (Applied Biosystems) using EvaGreen Dye (Biotium). For analysis of the VEGF mRNA levels, we used 5′-AAGGAGGAGGGCAGAATCATC-3′ as the upstream primer and 5′-GATCCGCATAATCTGCATGGT-3′ as the downstream primer, as well as 5′-AGGGCTGCTTTTAACTCTGGT-3′ and 5′-CCCCACTTGATTTTGGAGGGA-3′ for GAPDH. The relative

 

expression of VEGF mRNA was calculated using the $2^{-\Delta CT}$ method, in which $\Delta CT = CT_{VEGF} - CT_{GAPDH}$. All qRT-PCR reactions were performed in triplicate.

## Acknowledgements

We gratefully appreciate the support from the National Basic Research Program (2011CB933502) of China, the International S&T Cooperation Projects of China (2010DFA42060), and the National Natural Science Foundation (21020102038, 21121091).

## Notes and references

1 S. H. Kim, J. H. Jeong, T. Kim, S. W. Kim and D. A. Bull, *Mol. Pharmaceutics*, 2009, **6**(3), 718.
2 M. T. McManus, B. B. Haines, C. P. Dillon, C. E. Whitehurst, L. V. Parijs, J. Chen and P. A. Sharp, *Nat. Rev. Genet.*, 2002, **3**, 737.
3 Y. Dorsett and T. Tuschl, *Nat. Rev. Drug Discovery*, 2004, **3**, 318.
4 A. D. Fougerolles, H. Vornlocher, J. Maraganore and J. Lieberman, *Nat. Rev. Drug Discovery*, 2007, **6**, 443.
5 D. M. Dykxhoorn and J. Lieberman, *Cell*, 2006, **126**, 231.
6 J. Soutschek, A. Akinc, B. Bramlage, K. Charisse, R. Constien, M. Donoghue, S. Pandey, T. Racie, K. G. Rajeev, I. Rohl, I. Toudjarska, G. Wang, S. Wuschko, D. Bumcrot, V. Koteliansky, S. Limmer, M. Manoharan and H. P. Vornlocher, *Nature*, 2004, **432**, 173.
7 P. X. Guo, O. Coban, N. M. Snead, J. Trebley, S. Hoeprich, S. C. Guo and Y. Shu, *Adv. Drug Delivery Rev.*, 2010, **62**, 650.
8 K. A. Whitehead, R. Langer and D. G. Anderson, *Nat. Rev. Drug Discovery*, 2009, **8**, 129.
9 J. J. Shi, A. R. Votruba, O. C. Farokhzad and R. Langer, *Nano Lett.*, 2010, **10**, 3223.
10 J. J. Shi, Z. Y. Xiao, A. R. Votruba, C. Vilos and O. C. Farokhzad, *Angew. Chem., Int. Ed.*, 2011, **50**, 7027.
11 A. Aigner, *Curr. Opin. Mol. Ther.*, 2007, **9**, 345.
12 A. Muratovska and M. R. Eccles, *FEBS Lett.*, 2004, **558**, 63.
13 R. M. Schiffelers, A. Ansari, J. Xu, Q. Zhou, Q. Tang, G. Storm, G. Molema, P. Y. Lu, P. V. Scaria and M. C. Woodle, *Nucleic Acids Res.*, 2004, **32**, e149.
14 K. Itaka, N. Kanayama, N. Nishiyama, W. D. Jang, Y. Yamasaki, K. Nakamura, H. Kawaguchi and K. Kataoka, *J. Am. Chem. Soc.*, 2004, **126**, 13612.
15 Z. Medarova, W. Pham, C. Farrar, V. Petkova and A. Moore, *Nat. Med.*, 2007, **13**, 372.
16 A. M. Derfus, A. A. Chen, D. H. Min, E. Ruoslahti and S. N. Bhatia, *Bioconjugate Chem.*, 2007, **18**, 1391.
17 A. Elbakry, A. Zaky, R. Liebl, R. Rachel, A. Goepferich and M. Breunig, *Nano Lett.*, 2009, **9**, 2059.
18 L. Qi and X. Gao, *Expert Opin. Drug Delivery*, 2008, **5**, 263.
19 R. Bakalova, Z. Zhelev, H. Ohba and Y. Baba, *J. Am. Chem. Soc.*, 2005, **127**, 11328.
20 A. A. Chen, A. M. Derfus, S. R. Khetani and S. N. Bhatia, *Nucleic Acids Res.*, 2005, **33**(22), e190.
21 L. F. Qi and X. H. Gao, *ACS Nano*, 2008, **2**(7), 1403.
22 J. O. McNamara, E. R. Andrechek, Y. Wang, K. D. Viles, R. E. Rempel, E. Gilboa, B. A. Sullenger and P. H. Giangrande, *Nat. Biotechnol.*, 2006, **24**(8), 1005.
23 V. Bagalkot and X. H. Gao, *ACS Nano*, 2011, **5**(10), 8131.
24 D. H. Shangguan, Y. Li, Z. W. Tang, Z. C. Cao, H. W. Chen, P. Mallikaratchy, K. Sefah, C. J. Yang and W. H. Tan, *Proc. Natl. Acad. Sci. U. S. A.*, 2006, **103**, 11838.
25 D. H. Shangguan, Z. W. Tang, P. Mallikaratchy, Z. Y. Xiao and W. H. Tan, *ChemBioChem*, 2007, **8**, 603.
26 T. Vosch, Y. Antoku, J. C. Hsiang, C. I. Richards, J. I. Gonzalez and R. M. Dickson, *Proc. Natl. Acad. Sci. U. S. A.*, 2007, **104**, 12616.
27 N. de Souza, *Nat. Methods*, 2007, **4**, 540.
28 J. J. Li, X. Q. Zhong, F. F. Cheng, J. R. Zhang, L. P. Jiang and J. J. Zhu, *Anal. Chem.*, 2012, **84**(9), 4140.
29 T. C. Chu, K. Y. Twu, A. D. Ellington and M. Levy, *Nucleic Acids Res.*, 2006, **34**(10), e73.
30 V. Dapic, V. Abdomerovic, R. Marrington, J. Peberdy, A. Rodger, J. O. Trent and P. J. Bates, *Nucleic Acids Res.*, 2003, **31**(8), 2097.
31 N. Li, J. N. Ebright, G. M. Stovall, X. Chen, H. H. Nguyen, A. Singh, A. Syrett and A. D. Ellington, *J. Proteome Res.*, 2009, **8**(5), 2438.
32 C. I. Richards, S. Choi, J. C. Hsiang and Y. Antoku, *J. Am. Chem. Soc.*, 2008, **130**, 5038.
33 W. W. Guo, J. P. Yuan, Q. Z. Dong and E. K. Wang, *J. Am. Chem. Soc.*, 2010, **132**, 932.
34 J. T. Petty, J. Zhang, N. V. Hud and R. M. Dickson, *J. Am. Chem. Soc.*, 2004, **126**, 5207.
35 J.-L. Bridot, A.-C. Faure, S. Laurent, C. Riviere, C. Billotey, B. Hiba, M. Janier, V. Josserand, J.-L. Coll, L. V. Elst, R. Muller, S. Roux, P. Perriat and O. Tillement, *J. Am. Chem. Soc.*, 2007, **129**, 5076.
36 A. P. Alivisators, K. P. Johnsson, X. Peng, T. E. Wilson, C. J. Loweth, M. P. Bruchez Jr and P. G. Schultz, *Nature*, 1996, **382**, 609.
37 D. S. Seferos, A. E. Prigodich, D. A. Giljohann, P. C. Patel and C. A. Mirkin, *Nano Lett.*, 2009, **9**(1), 308.
38 Z. Liu, M. Winters, M. Holodniy and H. J. Dai, *Angew. Chem., Int. Ed.*, 2007, **46**, 2023.
39 V. Sokolova and M. Epple, *Angew. Chem., Int. Ed.*, 2008, **47**, 1382.
40 Z. S. Sun, Y. L. Wang, Y. T. Wei, R. Liu, H. R. Zhu, Y. Y. Cui, Y. L. Zhao and X. Y. Gao, *Chem. Commun.*, 2011, **47**, 11960.
41 Z. Y. Xiao, D. H. Shangguan, Z. H. Cao, X. H. Fang and W. H. Tan, *Chem.–Eur. J.*, 2008, **14**, 1769–1775.
42 S. W. Yang and T. Vosch, *Anal. Chem.*, 2011, **83**, 6935.
43 O. Bagasra and K. R. Prilliman, *J. Mol. Histol.*, 2004, **35**(6), 545–553.
44 J. H. Yu, S. Choi and R. M. Dickson, *Angew. Chem., Int. Ed.*, 2009, **48**, 318.
45 G. Y. Lan, C. C. Huang and H. T. Chang, *Chem. Commun.*, 2010, **46**, 1257.
46 Y. A. Shieh, S. J. Yang, M. F. Wei and M. J. Shieh, *ACS Nano*, 2010, **4**(3), 1433.
47 J. W. Guo, X. L. Gao, L. N. Su, H. M. Xia, G. Z. Cu, Z. Q. Pang, X. G. Jiang, L. Yao, J. Chen and H. Z. Chen, *Biomaterials*, 2011, **32**, 8010.
48 W. Li, X. H. Yang, K. M. Wang, W. H. Tan, Y. He, Q. P. Guo, H. X. Tang and J. B. Liu, *Anal. Chem.*, 2008, **80**, 5002.